Characterization of the failure shots of an induction voltage adder

Guo Fan, Wei Bing, Xie Weiping, Geng Lidong, Zou Wenkang, Xia Minghe, He An, Zhou Liangji, Zhao Yue, Yuan Jianqiang, and Wang Meng

Institute of Fluid Physics, China Academy of Engineering Physics, Mianyang 621900, China

(Received 14 June 2023; accepted 24 August 2023; published 6 September 2023)

The properties of the failure shots on an induction voltage adder are described. This induction voltage adder is composed of six identical prime pulsed power sources, six induction cavities, and a lossless vacuum insulation output transmission line which is terminated by a rod-pinch diode. The failure modes include too early and too late firing of the laser-triggered gas switch in the prime pulsed power sources and abnormal diode impedance declining. The amplitudes of the voltage pulses across the feed port and azimuthal transmission line of the induction cavity are increased by 38% and 48%, respectively, in the event that this cell is driven too early. On the contrary, a reverse voltage pulse will be produced at the induction cavity when it is fired too late. The peak value of the reverse voltage pulse is about 50% of that of the normal polarity pulse. The abnormal rod-pinch diode impedance declining taking place occasionally decreases the load voltage and x-ray dose remarkably. However, the average amplitude of the voltage pulses across the six induction cavities is almost the same as that of a normal shot. We have also analyzed the property of the voltage pulses across the induction cell under the circumstance that only one induction cavity is fired. Both the experimental and circuit simulation data suggest that in this case the voltage pulses on the induction cell are nearly identical even though the load impedance varies vastly.

DOI: 10.1103/PhysRevAccelBeams.26.090402

I. INTRODUCTION

Induction voltage adder (IVA) has been extensively employed to execute flash radiography and radiation effect qualification and testing [1–3]. At present, many IVAs are developed and operated for various research programs such as Hermes-III [4] machine for gamma-ray production, Radiographic Integrated Test Stand [5,6], Cygnus [7,8], Merlin [9], and Jianguang-II accelerator [10,11] for flash x-ray generation.

An IVA is usually composed of prime energy storage sections, pulse forming systems, and multi-induction-cavity connected in series by an output transmission line. For an ideal IVA, each induction cell must be driven at the time when the electromagnetic wave from the upstream sections arrives [12–14]. In this case, the voltage pulses across each cell are almost identical to each other. However, due to the random conduction times of the switches in the pulse-forming sections, the induction cavities are always unable to be fired synchronously with the speed at which the electromagnetic wave propagates through the output transmission line. Anomalous voltage waveforms will be produced across the induction cells and the summed voltages within the output transmission line will also be influenced [5,14,15]. The anomalous voltages resulting from the non-ideal driven sequence have been investigated previously by circuit simulation [5,15]. It is suggested that the induction cavity driven early will induce a higher voltage pulse across it than the nominal value, while the voltage pulse across the cell fired late becomes low and even a reverse polarity voltage pulse appears. The circuit simulation results also conclude that the peak voltage of the induction cell will be increased by 60% in case the cell is driven too early, and a reverse voltage pulse of 70% of the nominal pulse occurs if the cell is driven very late [5]. Whereas, the simulation results have never been approved by experimental data.

In recent years, we have developed an IVA which is named Hawkeye-I [16–18]. It consists of six identical individual prime pulsed power sources and six induction cells. A lossless vacuum insulation transmission line threading the induction cavities serves as the output transmission line which is terminated by a positive polarity rod-pinch diode (RPD). A maximum voltage of about 4.2 MV could be achieved on the RPD and the corresponding spot size and dose at 1 m of the x-ray source are 1.4 mm and 17.9 rad, respectively. The Hawkeye-I accelerator has already been performed more than 500 shots and over 98% of the shots are successful. Nevertheless, some failure shots have taken place such as prefire and late-fire of the laser-triggered gas switch (LTGS) in the pulse forming systems, and abnormal time history of the RPD impedance.

Published by the American Physical Society under the terms of the Creative Commons Attribution 4.0 International license. Further distribution of this work must maintain attribution to the author(s) and the published article's title, journal citation, and DOI.

We have also executed the experiments that only one induction cell was driven.

In this paper, the characteristics of the above-mentioned shots will be described. The remainder of this paper is organized as follows. In the following section we will give a brief description of the Hawkeye-I facility and the voltage and current diagnostics mounted throughout the machine will also be introduced. In Sec. III, the experimental results will be described. Section IV presents conclusions.

II. DESCRIPTION OF THE HAWKEYE-I FACILITY

Figure 1 shows the schematic view of the Hawkeye-I machine. Each prime pulsed power source is composed of an energy storage section, a tesla transformer, an intermediate storage capacitor (ISC), an LTGS, a pulse forming line (PFL), a self-breaking oil switch, and a water transmission line (WTL). Two 4 μF capacitors and a three-electrode gas switch located in the energy storage bank provide the primary energy of each pulsed power source. The conduction of the three-electrode gas switch is induced by a high-voltage pulse from a trigger unit. The output of the energy storage section is enhanced by a tesla transformer and charges the ISC whose capacitance and one-way transmit time are 13.4 nF and 53.6 ns, respectively. The ISC is switched out by an LTGS and then charges the PFL. The impedance and one-way transmit time of the PFL are 4 Ω and 27 ns, respectively. The self-breaking oil switch downstream of the PFL closes at the time when the voltage pulse across the PFL approaches its maximum, and then a high voltage pulse with fast rise is launched and propagates through the WTL of which the impedance and one-way transmit time are 7 Ω and 70 ns, respectively. The high voltage pulses produced by each prime pulsed power source are added within the output transmission line by the induction cells. The output line is designed neither in driver-matched mode nor in load-matched mode to avoid explosive electron emission which is the requirement of the preferred performance of the RPD. The impedances of the output transmission line corresponding to each induction cavity increase linearly from 20 Ω at the first cell to 70 Ω at the last cell. An RPD is employed at the end of the output transmission line to transform the electrical energy into an x-ray pulse. A more detailed description of the Hawkeye-I accelerator is presented in Ref [18].

On a typical shot, more than 60 gauges were employed to monitor the performance of Hawkeye-I. The voltage pulses on the ISCs and PFLs were diagnosed by D-dot monitors in the middle of the components. The conductions of the six-LTGS were monitored by differential-output B-dot sensors which produced the time derivative of the currents. The D-dot sensors mounted at the input ports of the WTLs gave the forward-going voltage waves transmitting in the WTLs. The D-dot and B-dot probes were also mounted in the induction cavities and output transmission line to examine their behaviors and the locations of the sensors are displayed in Fig. 2.

III. EXPERIMENTAL RESULTS

A. Only one induction cavity is driven

At the beginning of the commission of the Hawkeye-I facility, the six prime pulsed power sources have been tested individually. In this case, only one energy storage section was charged and initiated. Since the aqueous-electrolyte resistive load could be reused, it is employed downstream of the output transmission line instead of RPD. Figure 3 shows the measured voltage pulses at the feed port

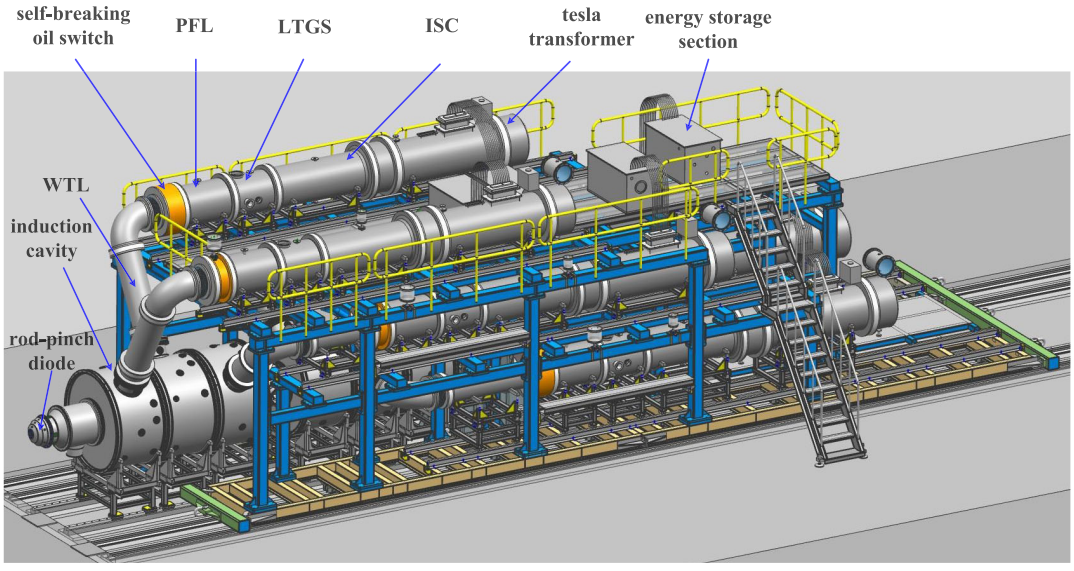

FIG. 1. Overview of the Hawkeye-I facility. The six prime pulsed power sources are divided into three layers, and each induction cell is driven by one pulsed power source.

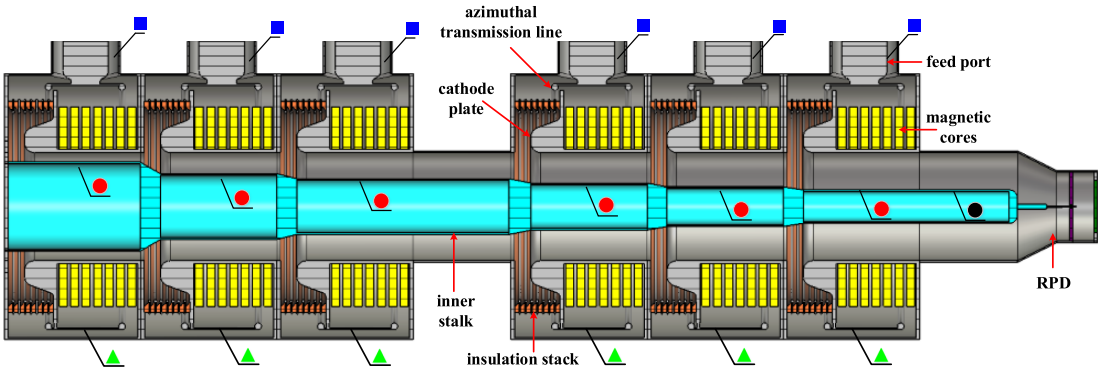

FIG. 2. Cross-sectional view of the induction cavities and output transmission line. The six induction cells from the left to right are labeled as No. 1 to No. 6, respectively. The main components of the induction cavity are the feed port, azimuthal transmission line, insulation stack, cathode plate, and magnetic cores. The inner stalk of the output transmission line is cantilevered and supported by a basement which is upstream of the No. 1 cavity and is not shown. The blue squares indicate the D-dot sensors for feed-port voltages measurement of each induction cell, and the green triangles denote the D-dot monitors to diagnose the azimuthal transmission line voltages of each cell. The red circles are the D-dot sensors for the detection of the output transmission line voltages. At each point, only one D-dot sensor is mounted. The black circle represents the locations of the D-dot and B-dot probes downstream of the last induction cavity which is about 45 cm from the load. Two D-dot sensors distributed symmetrically and a B-dot probe are fielded at this point.

and azimuthal transmission line of the No. 2 induction cell when only this cavity is driven. For this shot, the charging voltages of the capacitors in the energy storage bank are about ±55 kV. Figure 3 also shows the circuit simulation results under the same condition. Both the experimental and circuit simulation data suggest that the amplitude of the voltage pulse at the azimuthal transmission line is higher than that of the feed port section. Although the impedance of the aqueous-electrolyte resistive load varies vastly, the voltages across the No. 2 cavity are nearly identical during the entire pulse duration. Figure 4 presents the experimental and circuit simulation results when only the No. 5 induction cavity is fired. It is also demonstrated that the voltage pulses are almost independent of the load impedance. Figure 5 displays the circuit simulation results with a broad range of load impedance. The load impedance varies three orders of magnitude, however, the voltage pulses across the induction cell are nearly invariant except for slight differences at the falling edges parts. This phenomenon might be explained by the following truth. When only one induction cavity is driven the electromagnetic wave not only propagates toward the aqueous-electrolyte resistive load but also transmits to the other induction cells and upstream pulse-forming sections. In fact, a reverse voltage pulse will appear on the other cells and WTLs. This means that the other induction cells together with the aqueous-electrolyte resistive load serve as the actual load. Although the impedance of the resistive load changes evidently, the impedance of the actual load does not vary significantly.

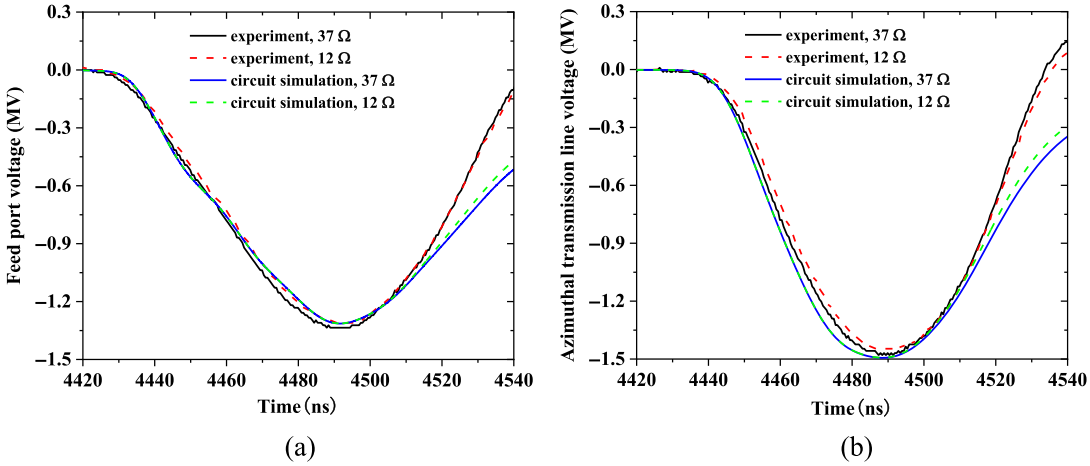

FIG. 3. (a) Feed port and (b) azimuthal transmission line voltages of No. 2 induction cavity. The amplitudes are about 1.32 and 1.48 MV, respectively. The black solid and red dash lines indicate the experimental results when the impedances of the aqueous-electrolyte resistive loads are 37 and 12 Ω, respectively. The blue solid and green dash lines denote the circuit simulation results.

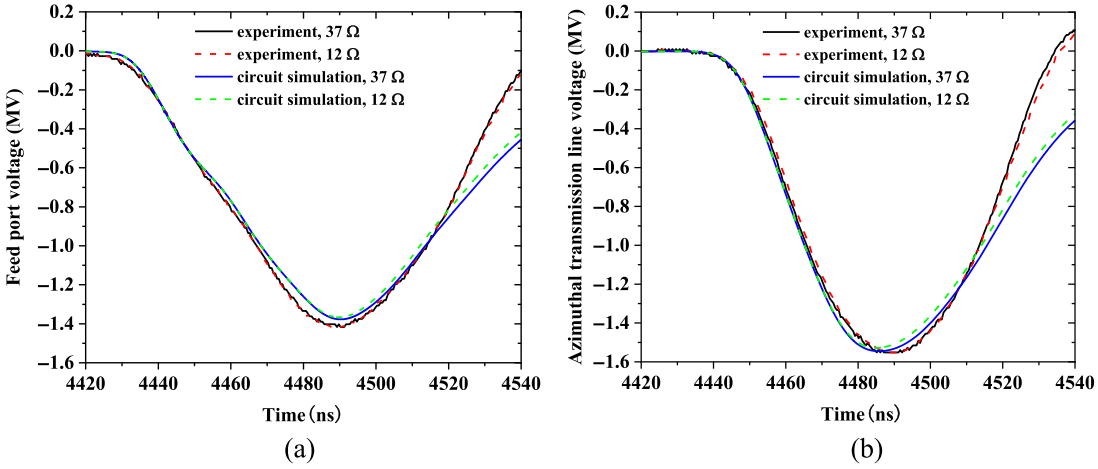

FIG. 4. (a) Feed port and (b) azimuthal transmission line voltages of No. 5 induction cavity. The peak values are about 1.4 and 1.54 MV, respectively. The black solid and red dash lines represent the experimental results when the impedances of the aqueous-electrolyte resistive loads are 37 and 12 Ω, respectively. The charging voltages are also about ±55 kV. The blue solid and green dashed lines indicate the circuit simulation results.

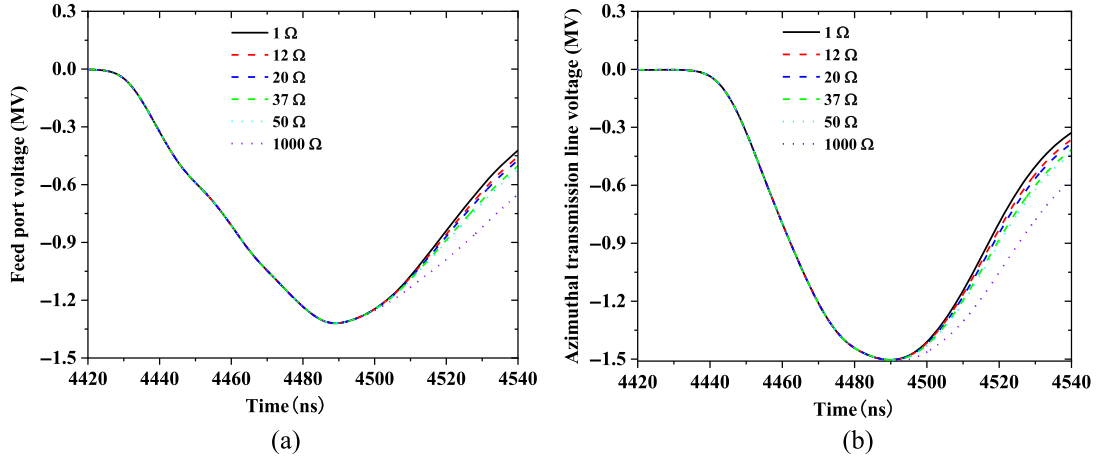

FIG. 5. (a) Feed port and (b) azimuthal transmission line voltages of No. 2 induction cavity with different load impedances given by circuit simulation.

B. Too early firing of the LTGS

LTGS has been frequently used in large-scale pulsed power machines to synchronize the current and/or voltage pulses produced by multimodule [19]. However, it usually constrains the reliable operation of the accelerator. Failure modes such as too early fire, too late fire, flashover, and great jitter resulting from deterioration of electrodes, optics, and insulators components take place occasionally [20].

Shot 94 is a failure since the No. 6 LTGS closes before the command laser beam triggers. For this shot, an RPD is employed instead of the above-mentioned aqueous-electrolyte resistive load. The RPD is made up of a tungsten anode rod and an aluminum cathode plate with an annular aperture at its central region. The diameters of the anode rod and cathode aperture are about 1.5 and 19 mm, respectively. The capacitors charging voltages of this shot are about ±60 kV. Figure 6 shows the normalized derivative of the conduction currents of the six-LTGS obtained during the experiment. It clearly indicates that the closure of the No. 6 LTGS is about 85 ns earlier than the other switches. The voltage pulses across the feed ports and azimuthal transmission lines of the six-cell of this shot are displayed in Fig. 7. It is shown that only the No. 6 induction cell is fired during most time of the initial pulse duration and the peak values of the voltage pulses across this cell are much higher than those of the other cavities. The amplitudes of the voltage pulses at the feed port and azimuthal transmission line of the No. 6 cavity are about 1.45 and 1.72 MV, respectively, while the average peak values of the voltage pulses at the feed ports and azimuthal transmission lines of the other cells are only about 1.04 and 1.13 MV, respectively.

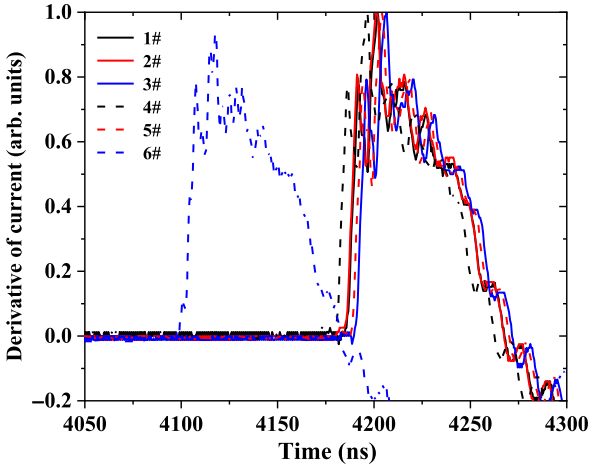

FIG. 6. Normalized derivative of the currents flowing through the six-LTGS measured by B-dot sensors of shot 94. The LTGS is labeled according to the corresponding induction cell.

We have examined eight normal shots at the same operation conditions as shot 94. Due to the jitters of six-LTGS and self-breaking oil switches, the driven sequences of the six induction cells of the eight shots change from shot to shot. This leads to the variation of the voltage pulse across each cell. However, none of the induction cavity is fired too early or too late and a nearly nominal load voltage could be achieved. The average amplitudes of the voltage pulses at the feed ports and azimuthal transmission lines of all six cells of the eight shots are about 1.05 and 1.16 MV, respectively. It could be concluded that the peak values of the voltage pulses across the feed port and azimuthal transmission line will be increased by about 38% and 48%, respectively, if the induction cell is driven 85 ns earlier than the other cavities.

Significant increase of the operating voltage may be due to that the topology of the IVA could be modeled by a Thevenin equivalent circuit [21]. The prime pulsed power source will develop a voltage near its open-circuit value across the corresponding induction cell, and the electromagnetic waves from the other cells induce a reverse voltage pulse and degrade the voltage across this cell to the nominal value. This means the voltage across the induction cavity is not solely determined by the corresponding pulsed power source that drives it but is also dependent on the other pulsed power sources. If an induction cell is fired much early before the reverse voltage pulse arrives, the near open-circuit voltage could be developed in the intervening time [5,14].

Since too early firing of the LTGS is unavoidable the induction cell should be able to withstand the anomalous voltage of this case. The insulation stack, azimuthal transmission line, and cathode plate of the induction cavity should be designed with a suitable margin to tolerate such anomalous stress. The experimental data displayed in Fig. 7 also suggest that the amplitudes of the positive polarity voltage pulses across the No. 1 to No. 5 induction cells are very low. The stress under this circumstance is unnecessary to take into additional consideration.

C. Too late firing of the LTGS

Shot 148 is also a failure since the No. 2 LTGS closes too late. The RPD with the same configuration as that of shot 94 is employed and the charging voltages are about ±55 kV for this shot. The normalized derivative of the six-LTGS conduction currents are presented in Fig. 8. It is seen that the closure of the No. 2 LTGS is about 70 ns later than the other switches. Figure 9 displays the voltages across the feed ports and azimuthal transmission lines of the six induction cavities of shot 148. The voltage pulses on the late-driven cell are in positive polarity while the stresses across the other cells are in negative polarity. The average amplitudes of the voltage pulses across the feed ports and azimuthal transmission lines of the normal-driven cavities are about 1.04 and 1.20 MV, respectively, and the peak values of the positive polarity voltage pulses at the corresponding sections of the late-driven cell are about

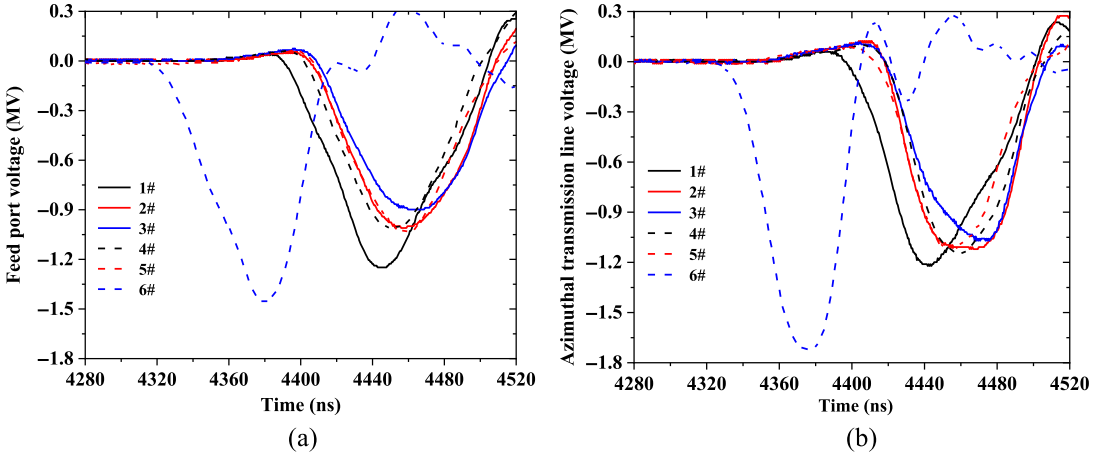

FIG. 7. (a) Feed ports and (b) azimuthal transmission lines voltages of shot 94 by experiment.

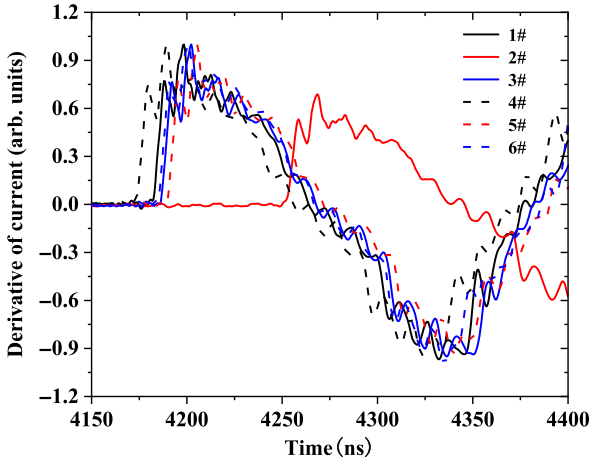

FIG. 8. Normalized derivative of the currents flowing through the six-LTGS measured by B-dot monitors of shot 148.

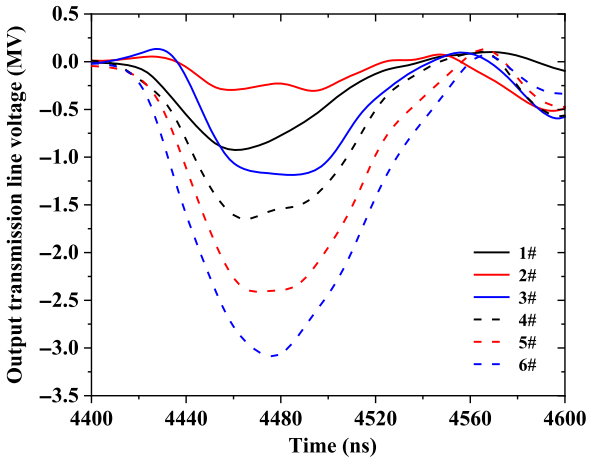

FIG. 10. Output transmission line voltages of shot 148. The labels in the plot are the same as the Nos. of the induction cavities.

0.55 and 0.65 MV, respectively. The amplitudes of the reverse voltage pulses are nearly 53% of those of the nominal negative voltage pulses. The voltage waveforms of this shot from the D-dot sensors mounted on the inner electrode of the output transmission line are shown in Fig. 10. Since the No. 2 induction cell is driven too late the energy produced by the other prime pulsed power sources will transmit to the No. 2 cell and upstream WTL. Therefore, the amplitude of the output transmission line voltage at the No. 2 cavity is only 0.3 MV and much lower than that of the No. 1 cell which is about 0.93 MV.

The insulation stack in the induction cavity is composed of multilayer 45° insulator rings separated by grading rings. However, the breakdown stress of the insulator ring is polarity dependent. Its orientation is designed to withstand the normal negative voltage pulse and the breakdown field of the positive pulse is much lower than that of the negative one [22–24]. Fortunately, it was demonstrated in the DARHT-2 program that the reverse stresses up to 50% had little effect [5]. The reverse voltage pulse across the insulation stack resulting from the too late firing of the LTGS will not lead to a severe accident.

The breakdown field in the transformer oil is also related to the polarity of the voltage pulse. Its breakdown stress is usually assessed by the empirical formula proposed by Martin [25,26]

$$E_{+} = 0.48 t_{\mathrm{teff}}^{-1/3} A^{-0.075}, \tag{1}$$

$$E_{-} = 0.667 t_{\mathrm{teff}}^{-1/3} A^{-0.075} [1 + 0.12 (E_{\max}/E_{\mathrm{mean}} - 1)^{0.5}], \tag{2}$$

where E_{+} and E_{-} are the electric fields in MV/cm of which the positive and negative electrodes have a 50% probability of breakdown, respectively, t_{eff} is the effective pulse duration in μs for which the voltage is above 63% of the peak value, A indicates the stressed area where the electric field is above 90% of the maximum field in cm^2, $E_{\max}$ and E_{mean} are the peak and mean electric fields of the stressed

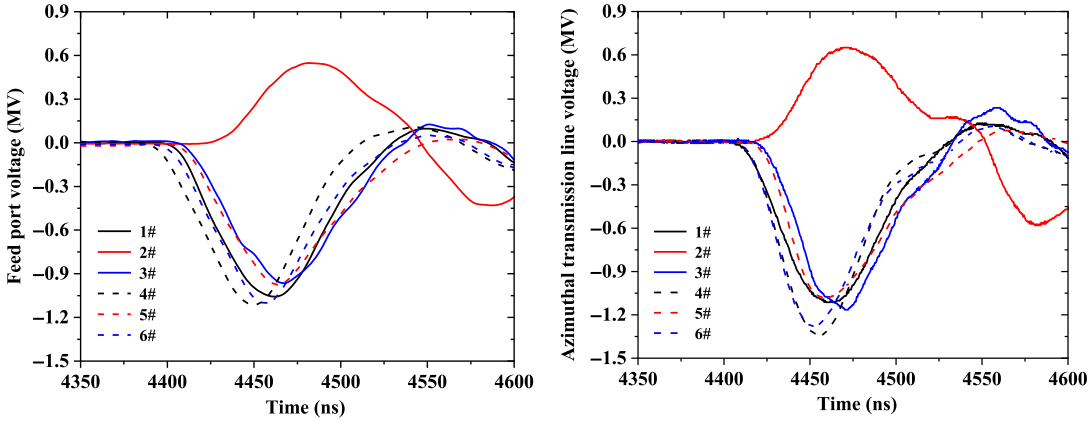

FIG. 9. (a) Feed ports and (b) azimuthal transmission lines voltages of shot 148 by experiment.

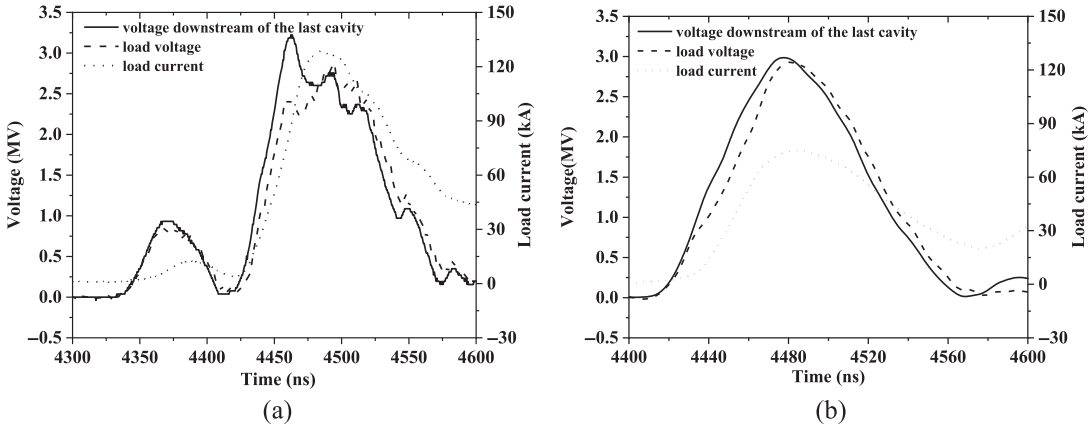

FIG. 11. Voltages downstream of the last cavity (black solid lines), load voltages (black dash lines), and load currents (black dot lines) of (a) shot 94 and (b) shot 148. The load voltages are determined by induction correction from the voltage pulses acquired by the D-dot sensors labeled as a black circle in Fig. 2. The currents at this point are regarded as the load currents straightforwardly. The x-ray doses at 1 m from the RPD monitored by LiF thermoluminescent dosimeters (TLDs) of shot 94 and shot 148 are 3.5 and 9.5 rad, respectively.

area, respectively, also in MV/cm. The azimuthal transmission line is immersed in the transformer oil. Its circular high-voltage electrode is at the negative potential and the induction cavity shell is the positive electrode. Because of the field distortions at the edges of the circular high-voltage electrode, the electric stresses within those regions are usually the highest [17]. According to the formulas mentioned above the breakdown field in the bulk of transformer oil will be decreased by nearly 40% if the circular high-voltage conductor converts to the positive electrode. Thus, the reverse stress up to 53% of the normal polarity pulse is also not a serious concern considering the transformer oil insulation safety.

The Hawkeye-I accelerator has been mainly used in hydrodynamic experiments to take stop-action images of the materials driven by explosives. Because the cost of the hydrodynamic experiments is always valuable, generation of the x ray at the desired timing reliable is crucial. Figure 11 gives the load voltages and load currents of shot 94 and shot 148. For shot 94 the RPD will be damaged by the initial pulse and the voltage pulses from the other prime pulsed power sources could not produce effective x ray. Moreover, the timing of the x ray is also earlier than the required moment. However, for shot 148 a slightly lower load voltage than the normal shot could still be achieved and the timing of the x ray also satisfies the requirement. The image of the explosive event could still be acquired despite of slightly inferior quality. Therefore, the fault mode of too late firing of the LTGS is preferred to too early firing.

D. Abnormal RPD impedance declining

The characteristic of the RPD is strongly dependent on the plasma's behaviors [27–29]. When the electric stress on the cathode plate exceeds the explosive electron emission threshold, the plasma will be produced on the cathode surface and the electron emission from the cathode will be initialized. After sufficient electrons flow toward the anode rod and enough energy is deposited, the temperature of the anode rod increases a lot. This leads to the contaminants on the anode surface desorption and subsequently ionization, and a plasma formation on the anode rod surface. The anode and cathode plasmas expand toward each other which decreases the effective ratio of the cathode to anode radii and consequently results in diode impedance decaying. For the RPD the majority of the x ray is produced during the magnetically limited flow regime in which the trajectories of the electrons emitting from the cathode are deflected by the magnetic field and pinched to the anode rod tip. The time history of the diode impedance during this regime is very crucial to the RPD performance.

The Hawkeye-I machine has already been performed more than 500 shots. We have discovered that for a few shots the peak values of the load voltages are lower than the normal shots but the load currents increase. It means that the impedances of the RPDs of these shots are sufficiently lower than the normal shots during the magnetically limited flow regime. Figure 12 shows the load voltages and currents of two consecutive shots. Not only the operation parameters of the pulsed power machine but also the configurations of the RPDs are the same for the two shots, and we do not perform any maintenance except for replacing the RPD after the first shot. Moreover, since the concentricity between the anode rod and cathode plate of the RPD influences the performance of the diode noticeably [18,30], an electrode concentricity evaluation system (ECES) is employed during the refurbishment of the diode. The ECES sets a camera in the front of the diode to capture the images of the anode rod and cathode plate which are displayed on a computer in real time. The cathode plate is adjusted to align with the anode rod by this guide. The eccentricities for the two shots are almost

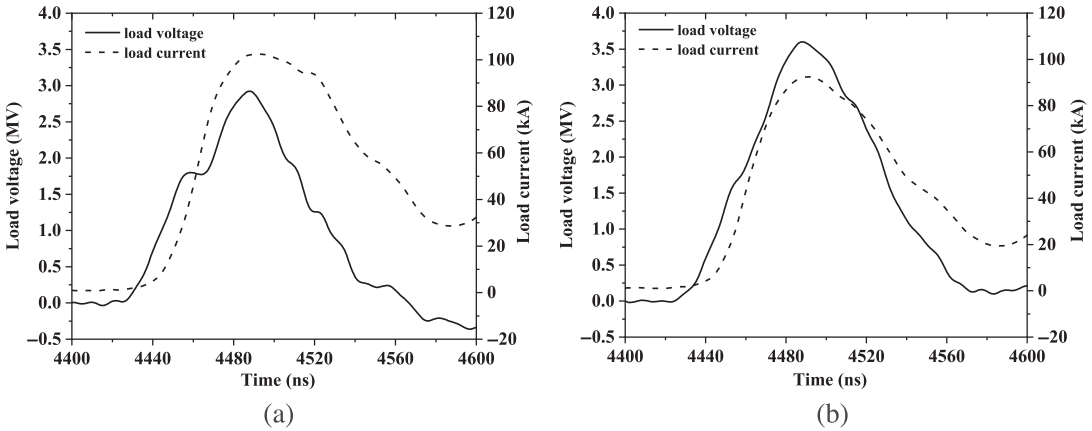

FIG. 12. Load voltages (black solid lines) and load currents (black dash lines) of (a) shot 189 and (b) shot 190. The load voltages are also decided by induction correction from the voltage pulses obtained downstream of the last induction cell. The charging voltages of the two shots are ±55 kV.

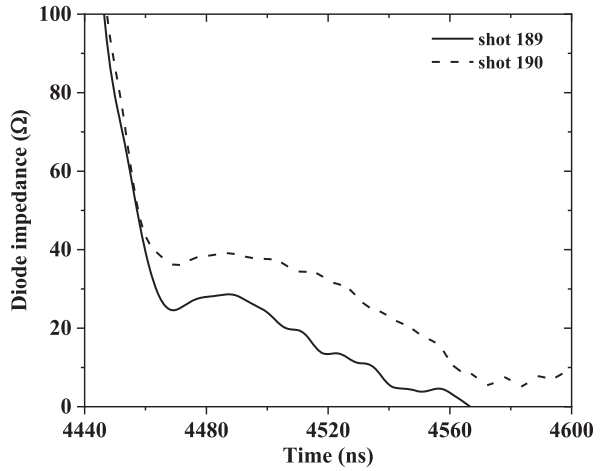

FIG. 13. Diode impedance profiles of shot 189 (solid line) and shot 190 (dash line).

the same and both are within 0.05 mm. However, the amplitudes of the load voltage and current pulses of shot 189 are 2.9 MV and 102.7 kA, respectively, while the peak values of shot 190 are 3.6 MV and 92.9 kA, respectively. The time histories of the diode impedances of the two shots are presented in Fig. 13. It is clearly seen that during most of the time the diode impedance of shot 190 is higher than that of shot 189. Consequently, the x-ray dose of shot 189 is only 7 rad and much lower than that of shot 190 which is about 13.7 rad. Figure 14 gives the voltage pulses at the feed ports of six induction cavities of shot 189 and shot 190. Although the voltages across the induction cells are different due to the nonideal driven sequence, the average peak values of the voltage pulses of the two shots are almost equal, 0.95 MV for shot 189 and 0.94 MV for shot 190.

The abnormal diode impedance declining might be attributed to the powder from the tungsten anode rod which adheres to the conductors nearby the diode region. Since the commission of the Hawkeye-I machine, the

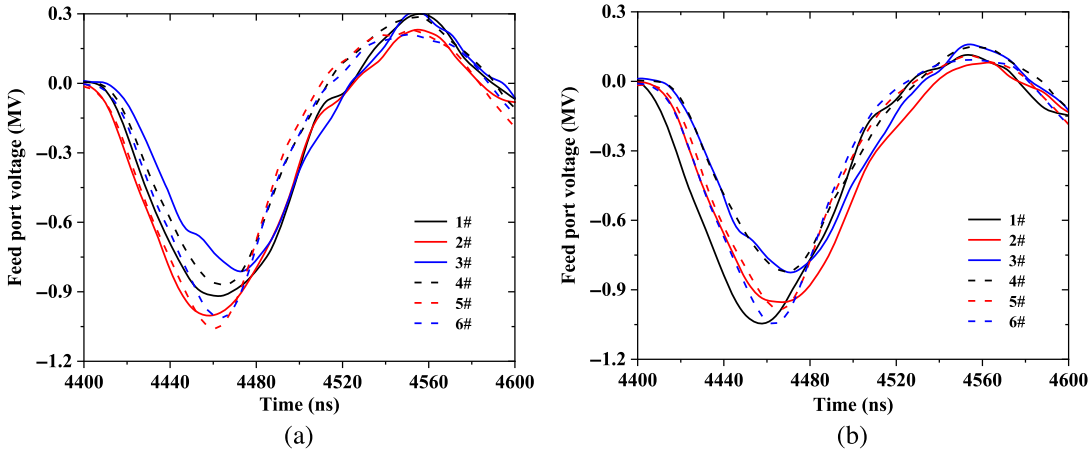

FIG. 14. Feed port voltages of (a) shot 189 and (b) shot 190. The average amplitudes of the voltage pulses of shot 189 and shot 190 are about 0.95 and 0.94 MV, respectively.

performances of the RPDs are regular for the initial 176 shots. However, after that abnormal shots have taken place occasionally. A fourth of the shots did not perform as expected from shot 177 to shot 192. Then, the outer electrode of the transmission line nearby the RPD is replaced by a new one and its inner conductor is cleaned with detergent. The abnormal shot does not take place for the upcoming 20 consecutive shots. We have optimized the experiment flow chart since then. The electrodes of the output transmission line downstream of the last induction cavity must be cleaned over each group of 20 shots. The abnormal diode impedance declining has never been observed again.

IV. CONCLUSIONS

We describe the characteristics of the voltage pulses across the induction cells under the circumstances that only one induction is driven, too early and too late firing of the LTGS, and abnormal RPD impedance declining. It is demonstrated both by experimental and circuit simulation data that the voltage pulse across the induction cavity except for the falling edge is irrelevant to the load impedance when only this induction cell is driven. In case the induction cavity is fired too early the amplitudes of the voltage pulses across the feed port and azimuthal transmission line of the induction cell will be increased by about 38% and 48%, respectively. Since the electric stresses will also be enhanced a lot, this phenomenon should be taken into account carefully when designing the insulation safety of the induction cavity. Whereas, a reverse polarity voltage pulse will be produced if the induction cavity is driven too late. The peak value of the reverse polarity pulse is about 50% of the normal negative pulse. The abnormal RPD impedance declining will decrease the load voltage and x-ray dose a lot, but the electric stresses across the induction cavities are almost the same as those of the normal shots.

The magnetic cores in the induction cell are reset by a unipolar current pulse with a duration of about several milliseconds after finishing each shot. The operation points of the magnetic cores will be repositioned at the negative saturation induction $-B_s$ and relaxed to the negative remanent induction $-B_r$ after the end of the resetting pulse. The reverse voltage pulse resulting from the too late firing of the LTGS will induce the operation points of the magnetic cores moving along the hysteresis curve from $-B_r$ to $-B_s$. Therefore, the reverse voltage pulse across the induction cell is also related to the squareness ratio of the hysteresis loop (B_r/B_s) of the magnetic cores. Note that the magnetic cores made up of 2605SA1 amorphous alloy ribbons are employed in our induction cavity instead of the conventional 2605Co material used in other cells. Since the induced anisotropy energy of 2605SA1 is much smaller than that of 2605Co, the remanent induction of the magnetic core from 2605SA1 material is very sensitive to the mechanical stress forming in the fabrication process [17,31–33]. The remanent inductions of the magnetic cores in our induction cavity are only about one-half of their saturation inductions while the squareness ratios of the hysteresis loops of the magnetic cores from 2605Co are usually greater than 0.9. Therefore, the experimental data of too late firing of the LTGS presented herein may not be consistent with the results of the IVA such as RITS [5] and Merlin [9] employing the 2605Co as the magnetic core material.

Besides the failure modes described in this paper, the prefire of a three-electrode gas switch in the energy storage bank, malfunction of a laser facility, and flashover occurring over the interface between the plastic diaphragm and water in an ISC have also taken place. For all those shots, the PFL could not be charged normally and the forward-going voltage wave in the WTL is absent. The induction cell behaves like the condition of the too late firing of the LTGS.

ACKNOWLEDGMENTS

This work was supported by the National Natural Science Foundation of China (Grants No. 51907181 and No. 51977201).

[1] J. Maenchen, G. Cooperstein, J. O'Malley, and I. Smith, Advances in pulsed power-driven radiography systems, Proc. IEEE **92**, 1021 (2004).

[2] R. Delaunay, B. Cadilhon, L. Courtois, I. Mousseau, J. M. Plewa, C. M. Alvinerie, B. Cassany, C. Vermare, T. D'Almeida, M. Ribière, and R. Maisonny, Dual-pulse generation from a velvet cathode with a new inductive voltage adder for x-ray flash radiography applications, Phys. Rev. Accel. Beams **25**, 060401 (2022).

[3] J. A. Halbleib, T. W. L. Sanford, and J. W. Poukey, Radiation environment of Hermes III, IEEE Trans. Nucl. Sci. **35**, 1282 (1988).

[4] J. J. Ramirez, K. R. Prestwich, E. L. Burgess, J. P. Furaus, R. A. Hamil, D. L. Johnson, T. W. L. Sanford, L. O. Seamons, L. X. Schneider, and G. A. Zawadzkas, The Hermes-III program, in *Proceedings of the Pulsed Power Conference, Arlington* (IEEE, New York, 1987).

[5] I. D. Smith, V. L. Bailey, J. J. Fockler, J. S. Gustwiller, D. L. Johnson, J. E. Maenchen, and D. W. Droemer, Design of a radiographic integrated test stand (RITS) based on a voltage adder, to drive a diode immersed in a high magnetic field, IEEE Trans. Plasma Sci. **28**, 1653 (2000).

[6] N. Bruner, T. Genoni, E. Madrid, D. Rose, D. Welch, K. Hahn, J. Leckbee, S. Portillo, B. Oliver, V. Bailey, and D. Johnson, Modeling particle emission and power flow in pulsed-power driven, nonuniform transmission lines, Phys. Rev. ST Accel. Beams **11**, 040401 (2008).

[7] D. Weidenheimer, P. Corcoran, R. Altes, J. Douglas, H. Nishimoto, I. Smith, R. Stevens, D. L. Johnson, R. White, J. Gustwiller, J. E. Maenchen, P. Menge, R. Carlson, R. D. Fulton, G. Cooperstein, D. Droemer, and E. Hunt, Design of a driver for the Cygnus x-ray source, in *Proceedings of*

the 13th IEEE International Pulsed Power Conference, Las Vegas (IEEE, New York, 2001).

[8] J. R. Smith, M. R. Garcia, E. C. Ormond, M. F. Parrales, P. A. Flores, K. W. Hogge, S. R. Huber, S. E. Mitchell, J. R. Perez, T. A. Romero, and H. V. Truong, Cygnus performance on Vega, Los Alamos National Laboratory Technical Report No. LA-UR-18-24549, 2018.

[9] K. Thomas *et al.*, The MERLIN induction voltage adder radiographic accelerator, in *Proceedings of the 2017 IEEE 21st International Conference on Pulsed Power, Brighton* (IEEE, New York, 2017).

[10] H. Wei, J. H. Yin, P. F. Zhang, F. J. Sun, A. C. Qiu, T. X. Liang, J. T. Zeng, X. F. Jiang, Z. G. Wang, J. Sun, W. Y. Liu, Q. F. Luo, W. D. Ding, and Y. X. Hu, Development of a 4-MV, 80-kA-induction voltage adder for flash x-ray radiography, IEEE Trans. Plasma Sci. **47**, 5030 (2019).

[11] H. Wei, J. H. Yin, P. F. Zhang, F. J. Sun, A. C. Qiu, T. X. Liang, X. F. Jiang, Z. G. Wang, J. Sun, Q. F. Luo, H. L. Yang, W. B. Yao, H. Y. Jiang, and H. Y. Wu, Simulation, experiment, and performance of a 4 MV induction voltage adder machine for flash x-ray radiography, Phys. Rev. Accel. Beams **24**, 020402 (2021).

[12] I. Smith, P. Corcoran, V. Carboni, V. Bailey, H. Kishi, D. L. Johnson, J. Maenchen, I. Molina, R. Carlson, D. Fulton, K. Hahn, J. Smith, D. Droemer, K. Thomas, M. Phillips, S. Croxon, R. Forgan, and I. D. Smith, Induction voltage adder architectures and electrical characteristics, in *Proceedings of the 14th IEEE International Pulsed Power Conference, Dallas* (IEEE, New York, 2003).

[13] J. J. Ramirez, K. R. Prestwich, and I. D. Smith, Highpower, short-pulse generators based on induction voltage adders, Proc. IEEE **80**, 946 (1992).

[14] I. D. Smith, Induction voltage adders and the induction accelerator family, Phys. Rev. ST Accel. Beams **7**, 064801 (2004).

[15] T. A. Holt, R. J. Allen, R. C. Fisher, R. J. Commisso, and D. L. Johnson, Analysis of switch performance on the mercury pulsed-power generator, in *Proceedings of the 2005 IEEE Pulsed Power Conference, Monterey* (IEEE, New York, 2005).

[16] F. Guo, W. K. Zou, B. Y. Gong, J. H. Jiang, L. Chen, M. Wang, and W. P. Xie, Modeling power flow in the induction cavity with a two dimensional circuit simulation, Phys. Rev. Accel. Beams **20**, 020401 (2017).

[17] F. Guo, W. P. Xie, Z. Wang, J. H. Jiang, M. H. Xia, B. Wei, S. P. Feng, Y. Zhao, J. J. Kang, M. Wang, W. K. Zou, and L. Chen, Design of a 1-MV induction cavity and validation of the two-dimensional circuit model, Phys. Rev. Accel. Beams **22**, 020401 (2019).

[18] W. P. Xie *et al.*, Design and performance of a pulsed power-driven x-ray source for flash radiography, Phys. Rev. Accel. Beams **24**, 110401 (2021).

[19] J. J. Deng *et al.*, From concept to reality-A review to the primary test stand and its preliminary application in high energy density physics, Matter Radiat. Extremes **1**, 48 (2016).

[20] K. R. LeChien, M. E. Savage, V. Anaya, D. E. Bliss, W. T. Clark, J. P. Corley, G. Feltz, J. E. Garrity, D. W. Guthrie, K. C. Hodge, J. E. Maenchen, R. Maier, K. R. Prestwich, K. W. Struve, W. A. Stygar, T. Thompson, J. Van Den Avyle, P. E. Wakeland, Z. R. Wallace, and J. R. Woodworth, Development of a 5.4 MV laser triggered gas switch for multimodule, multimegampere pulsed power drivers, Phys. Rev. ST Accel. Beams **11**, 060402 (2008).

[21] R. J. Allen, R. J. Commisso, G. Cooperstein, P. F. Ottinger, and J. W. Schumer, Extension of the operating point of the Mercury IVA from 6 to 8 MV, in *Proceedings of the 2011 IEEE Pulsed Power Conference, Chicago, IL, USA* (IEEE, New York, 2011).

[22] W. A. Stygar *et al.*, Improved design of a high-voltage vacuum-insulator interface, Phys. Rev. ST Accel. Beams **8**, 050401 (2005).

[23] I. D. Smith, P. A. Corcoran, W. A. Stygar, T. H. Martin, R. B. Spielman, and R. W. Shoup, Design criteria for the Z vacuum insulator stack, in *Proceedings of the 11th IEEE International Pulsed Power Conference, Baltimore* (IEEE, New York, 1997).

[24] I. Smith, Flashover of vacuum interfaces with many stages, and large transit times, in *Proceedings of the IEEE Transactions on Plasma Science, Albuquerque* (IEEE, New York, 1995).

[25] J. C. Martin, Nanosecond pulse techniques, Proc. IEEE **80**, 934 (1992).

[26] R. J. Adler, Pulse Power Formulary, North Star Research Corporation (2002), http://www.highvoltageprobes.com/downloads.

[27] G. Cooperstein, J. R. Boller, R. J. Commisso, D. D. Hinshelwood, D. Mosher, P. F. Ottinger, J. W. Schumer, S. J. Stephanakis, S. B. Swanekamp, B. V. Weber, and F. C. Young, Theoretical modeling and experimental characterization of a rod-pinch diode, Phys. Plasmas **8**, 4618 (2001).

[28] F. C. Young, R. J. Commisso, R. J. Allen, D. Mosher, S. B. Swanekamp, and G. Cooperstein, F. Bayol, P. Charre, A. Garrigues, C. Gonzales, F. Pompier, and R. Vezinet, Rod pinch diode operation at 2 to 4 MV for high resolution pulsed radiography, Phys. Plasmas **9**, 4815 (2002).

[29] P. R. Menge, D. L. Johnson, J. E. Maenchen, D. C. Rovang, B. V. Oliver, D. V. Rose, and D. R. Welch, Optimization of a rod pinch diode radiography source at 2.3 MV, Rev. Sci. Instrum. **74**, 3628 (2003).

[30] L. D. Geng, Y. He, J. Q. Yuan, M. H. Wang, L. B. Cao, S. P. Feng, and W. P. Xie, Study on eccentricity effects of the rod-pinch diode radiography source, Rev. Sci. Instrum. **90**, 023304 (2019).

[31] C. H. Smith, Magnetic pulse compression by metallic glasses, J. Appl. Phys. **64**, 6032 (1988).

[32] G. E. Fish, Soft magnetic materials, Proc. IEEE **78**, 947 (1990).

[33] C. H. Smith, B. N. Turman, and H. C. Harjes, Insulations for metallic glasses in pulse power systems, IEEE Trans. Electron Devices **38**, 750 (1991).